International Journal of Plasticity xxx (2017) 1–14

Contents lists available at ScienceDirect

International Journal of Plasticity

journal homepage: www.elsevier.com/locate/ijplas

Slip transfer and deformation structures resulting from the low cycle fatigue of near-alpha titanium alloy Ti-6242Si

Sudha Joseph, Ioannis Bantounas, Trevor C. Lindley, David Dye*

Department of Materials, Royal School of Mines, Imperial College, Prince Consort Road, London SW7 2BP, UK

ARTICLE INFO

Article history:
Received 6 July 2017
Received in revised form 20 September 2017
Accepted 20 September 2017
Available online xxx

Keywords:
Titanium alloys
Transmission electron microscopy
Slip transmission
Fatigue
Dislocations

ABSTRACT

Near-alpha titanium alloy Ti6242Si, widely used in aero-engine compressor discs, was subjected to low cycle fatigue loading at room temperature. Fracture initiated by facet formation, followed by striated fatigue crack growth prior to final failure. Deformation occurred primarily by planar slip, localized into slip bands in the primary alpha. Within soft-oriented grains in a microtextured region, pile-up of a slip band within one grain resulted in the direct transfer of slip into an adjacent similarly oriented grain. In contrast, pile up of dislocations in a soft grain with a 'hard' oriented neighbour resulted in the activation of few non-connected dislocations in the hard grain, with <a>-type dislocations being activated and the observation of cross-slip. Whilst a high density of dislocations was present from precipitation of secondary alpha in the retained beta ligaments, a little dislocation interaction was observed between the transformed beta and the primary alpha grains.

© 2017 The Authors. Published by Elsevier Ltd. This is an open access article under the CC BY license (http://creativecommons.org/licenses/by/4.0/).

1. Introduction

Near-α titanium alloys, such as Ti6242Si, are employed in high temperature aero-engine compressors due to their combination of specific toughness, creep resistance and microstructural stability at temperatures around 400-600 °C (Hall et al., 1973; Tien et al., 1973; Terlinde et al., 1983; Honnorat, 1996). Thus, they are not normally subjected to high stresses while at temperatures that are of concern for dwell fatigue, a phenomenon associated with planar slip and strain-rate sensitive load shedding between grains associated with holds in load of several minutes at <250 °C (Hack and Leverant, 1980; Tal-Gutelmacher and Eliezer, 2005; Tan et al., 2015). During a flight cycle, a component is exposed to a variety of loading regimes. High stresses in the low cycle fatigue regime may be experienced at the thrust peak associated with take-off, and for the rotor bore this may be at lower temperatures if long soak times on taxi are reduced in an attempt to reduce local ground level airport emissions, which can be problematic at high volume locations such as Heathrow in the UK. Such low temperature dwells might give a cause for concern regarding dwell fatigue. In contrast, other periods of high throttle setting will be at elevated temperatures where dwell effects are absent. These effects continue to compromise design (McBagonluri et al., 2005; Qiu et al., 2014) and hence are very important to understand. In this work, the low cycle fatigue behaviour of the alloy is investigated.

The fatigue behaviour of near-α alloys mainly depends on microstructural variables such as volume fraction of primary alpha (Shen et al., 2004), its morphology (Eylon and Hall, 1977; Kassner et al., 1999), whether the variant state is colony or

* Corresponding author.
E-mail address: david.dye@imperial.ac.uk (D. Dye).

https://doi.org/10.1016/j.ijplas.2017.09.012
0749-6419/© 2017 The Authors. Published by Elsevier Ltd. This is an open access article under the CC BY license (http://creativecommons.org/licenses/by/4.0/).

Please cite this article in press as: Joseph, S., et al., Slip transfer and deformation structures resulting from the low cycle fatigue of near-alpha titanium alloy Ti-6242Si, International Journal of Plasticity (2017), https://doi.org/10.1016/j.ijplas.2017.09.012

basketweave (Evans, 1987; Sinha et al., 2006a; Dunne et al., 2007a; Dunne and Rugg, 2008) and micro- and macro-texture (Evans and Bache, 1994; Bache et al., 1997a; Bache, 2003; Dunne et al., 2007b; Pilchak, 2014). Furthermore, it is believed that hard/soft grain pairs act as fatigue initiation sites (Dunne et al., 2007a, 2007b; Dunne and Rugg, 2008) and this occurs by the formation of near-{0002} facets near-perpendicular to the loading direction on grains poorly oriented for <a> slip ('hard grains'), due to load shedding by adjacent grains that are well oriented for prism <a> slip ('soft grains') (Bache et al., 1997b; Bache and Evans, 2003; Kirane and Ghosh, 2008; Anahid et al., 2011; Zheng et al., 2016a,b). However, these facets may, or may not, show evidence of plasticity, and are believed to grow over more than one fatigue cycle – i.e. they are not formed simply by cleavage.

Ti6242Si (Ti-6Al-2Sn-4Zr-2Mo-0.1Si, wt.%) is a two-phase alloy with soft α phase and regions of retained β phase containing fine scale secondary α, where plasticity is assumed to initiate in the primary alpha (α_p) grains. Dislocation generation and transport within a grain can then result (Lee et al., 1990a, 1990b) in: (1) incorporation of the piled-up dislocations in the grain boundary and subsequent decomposition into grain boundary dislocations, (2) direct transfer of piled up dislocations through a grain boundary into the neighbouring grain, (3) piled up dislocations slipping along the grain boundary plane, (4) transfer of a dislocation through the boundary with a residual dislocation left at the grain boundary and/or (5) dislocations being ejected back into the pile-up grain. These processes involve the dynamics of dislocation motion as well as the geometry of slip at grain boundaries (Lee et al., 1990a). Slip transfer across the grain boundary occurs when the following three conditions (Lee et al., 1990a) are satisfied: (1) The angle between the lines of intersection of the incoming and outgoing slip planes with the grain boundary plane should be minimized; (2) the resolved shear stress acting on the possible slip system in the adjoining grain should be maximized; (3) the magnitude of the Burgers vector of any grain boundary dislocation produced during slip transfer should be minimized. Other stress relieving mechanisms are possible when the slip systems of lower critical stress are not favourable.

Slip transfer is connected to fatigue behaviour insofar as a lack of slip transfer will be associated with the production of sufficient stress concentration to result in the initiation of a fatigue crack in an initiating grain; conversely, easy slip transfer without the production of interface defects and debris will result in homogenous plastic deformation. Therefore, micro- and macro-texture will influence fatigue crack initiation. Of importance will also be the micromechanical loading state – the compatibility of the elastic moduli and plasticity between the grains, and therefore the stress perturbations associated with discontinuities such as grain boundaries (Hasija et al., 2003; Dunne et al., 2007a; Venkatramani et al., 2007; Dunne and Rugg, 2008). Macrozones, that is, regions of common orientation inherited from the ~0.5 mm prior beta grains, have been particularly implicated in fatigue performance (Le Biavant et al., 2002; Germain et al., 2005, 2008; Gey et al., 2012), and there has been discussion that macrozones may act as large structural units that deform simultaneously (Evans and Bache, 1994; Bache et al., 1997a; Bache, 2003), with fatigue crack initiation occurring at the interface between hard-oriented and soft-oriented macrozones (Bantounas et al., 2009; Tympel et al., 2016).

In this work, the dislocation structures produced during low cycle fatigue loading in Ti6246Si are investigated in detail, using transmission electron microscopy, with the aim of elucidating how slip transfer and grain boundary interactions more generally may contribute to fatigue crack initiation and propagation. Ti-6242Si was chosen for study because it is a near-alpha alloy that can, in certain microstructural conditions and loading regimes, suffer from cold dwell fatigue and which has a relatively simple equiaxed primary alpha microstructure in a transformed β matrix consisting of secondary alpha laths separated by a thin layer of β phase.

2. Experimental description

Ti6242Si buttons with composition shown in Table 1 were produced by arc melting in low pressure Ar from high purity Ti sponge, elemental additions and TiO powder. Small amounts of Si and oxygen are added to the alloy for high temperature properties and strength respectively. The alloy was processed by rolling in both the β and $\alpha + \beta$ domains, recrystallized in the $\alpha + \beta$ domain at 950 °C for 5 h and air-cooled. The alloy was then aged at 593 °C for 8 h and air cooled to promote Ti_3Al precipitation. A recrystallization temperature of 45 °C below T_β was chosen in order to obtain a high volume fraction of primary α.

Mechanical tests were conducted using Mayes servohydraulic machines with Instron 8800 controllers. Static tensile tests were carried out on dog bone shaped samples at a strain rate of 10^{-3} s^{-1}. Low cycle fatigue (LCF) tests were carried out on cylindrical samples with a 2.9 mm diameter and a 15 mm long gauge length. The tests were performed using a trapezoidal waveform with a ramp up/down time of 1 s, a 1 s hold at maximum stress of 95% of yield stress and an R ratio of 0.05.

A Zeiss Auriga field emission gun scanning electron microscope (FEG-SEM) in secondary electron imaging mode was used for metallography and fractography. Electron back-scattered diffraction (EBSD) was used for orientation imaging microscopy

Table 1
Nominal chemical composition of the alloy (wt.%).

Element	Al	Zr	Sn	Mo	Si	Fe	O	Y	Ti
Wt.%	6.0	4.0	2.0	2.0	0.1	0.25	0.15	0.005	Balance

Please cite this article in press as: Joseph, S., et al., Slip transfer and deformation structures resulting from the low cycle fatigue of near-alpha titanium alloy Ti-6242Si, International Journal of Plasticity (2017), https://doi.org/10.1016/j.ijplas.2017.09.012

(OIM). Samples sectioned in a plane perpendicular to the loading direction were used for microscopy investigations. The samples for this analysis were prepared by following standard metallographic procedures.

The dislocation analysis on LCF samples was conducted using a JEOL JEM-2100F TEM/STEM with an accelerating voltage of 200 kV. Discs of 0.5 mm thick were cut from the gauge of the samples tested, normal to the loading direction, ground to a thickness of 100–150 μm using SiC paper and electropolished using 3% perchloric acid, 57% methanol and 40% butan 1-ol in a Tenupol at −40 °C and 24V.

3. Results & discussion

3.1. Initial microstructure

Fig. 1(a) shows the typical bimodal microstructure of the alloy with dark α_p in the transformed β. The α_p grains are equiaxed and homogeneously distributed in the transformed β. Dark secondary alpha (α_s) platelets can also be observed in the retained β. The volume fraction of α_p was 50% with 2–6 μm grain size. Figs. 1(b) and (c) show macrozones present in the alloy, highlighting a particular 'hard' [0002]||RD macrozone adjacent to a 'soft' [0002]⊥RD macrozone. The overall texture obtained from the large area EBSD scan showed a weak (0001) rolling texture, Fig. 1(d).

3.2. Mechanical test results

The typical tensile stress-strain behaviour of the alloy shows a 0.2% yield strength of about 875MPa and an elongation of about 9%. A maximum stress of 95% of yield stress was applied to the un-notched LCF test with a fatigue lifetime of 23,914 cycles. The SEM and TEM observations of this failed LCF sample are discussed in the following sections.

3.3. Fractography

Near-surface fatigue crack initiation was observed, with the initiation grains having the appearance of relatively smooth facets, Fig. 2. Four facets in the initiation region were examined by quantitative tilt fractography (Sinha et al., 2007) and electron backscatter diffraction (EBSD) to find the spatial orientation and crystallographic orientation of the facet plane normal, Table 2. Facets 1 and 2 are initiation facets with fracture plane normal oriented 17.3° and 47.6° to the loading direction. Their neighbouring facets, 3 and 4, are oriented around 40.4° and 42.9°. The (0002) plane normal of the initiation

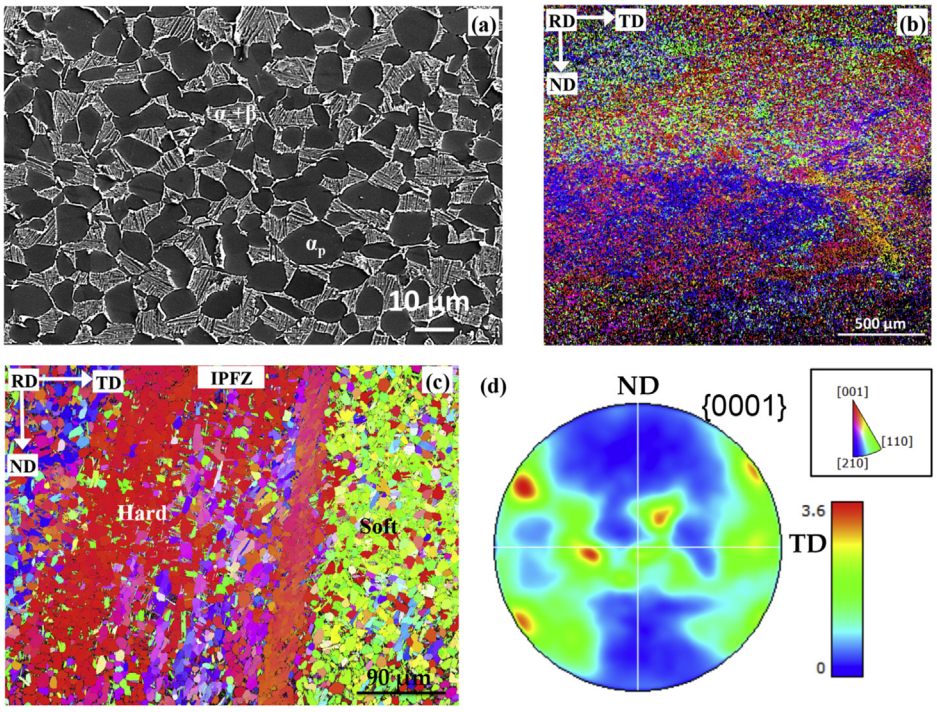


Fig. 1. (a) Bimodal microstructure of Ti 6242Si alloy, (b) large area EBSD scan illustrating the substantial macrozone size, (c) smaller area EBSD scan showing of a soft/hard macrozone combination. The IPF map is coloured according to the plane normal in the RD (out of the page). (d) (0001) pole figure of α_p phase obtained from the large area scan in (b).

Please cite this article in press as: Joseph, S., et al., Slip transfer and deformation structures resulting from the low cycle fatigue of near-alpha titanium alloy Ti-6242Si, International Journal of Plasticity (2017), https://doi.org/10.1016/j.ijplas.2017.09.012

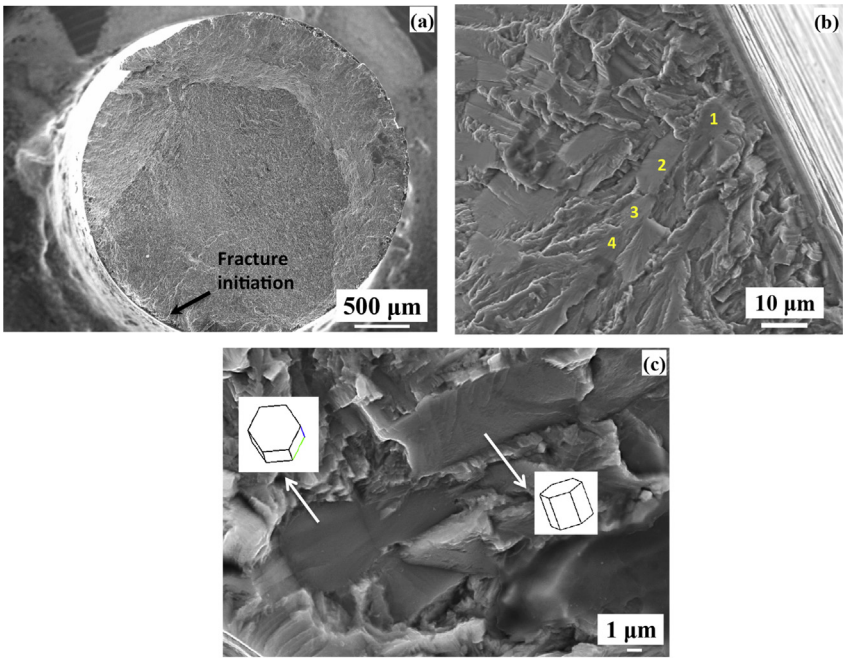


Fig. 2. SEM fractographs showing the (a) fracture surface with near surface fracture initiation (b) facet formation in the initiation region and (c) high-magnification view of the initiation facets.

facets were found respectively to be 15.3° and 44.8° to the loading direction, whilst the other two neighbouring facets were about 24° and 16.3°, so the average facet planes are close to, but not precisely low-index (0002) crystallographic planes. Other workers have reported similarly that fatigue facets were found to form oriented 0-16° to the basal plane (Davidson and Eylon, 1980) and 5° to the basal plane (Sinha et al., 2006b). In contrast, Davidson et al. (Davidson and Eylon, 1980) also observed pure basal facets in some Ti alloy fatigue specimens. Thus, terming these near-planar features facets should not be taken to imply that they formed in a single fatigue cycle by cleavage in a single event. Other features observed on the fracture surface are also shown in Fig. 3. Fig. 3(a) shows the facets adjacent to the initiation facets. Crack initiation was followed by crack growth with fatigue striations (Fig. 3b), secondary cracking (Fig. 3c) and finally sample failure by ductile microvoid coalescence (Fig. 3d).

3.4. Transmission electron microscopy

3.4.1. Slip transfer between soft grains

TEM analysis of samples extracted from the gauge section of the LCF specimens was carried out in the two beam condition under different beam directions to identify the dislocation Burgers vectors using the invisibility criterion, along with a trace analysis to identify the slip planes and dislocation types. The alloy was found to mainly deform by planar slip in α_p grains. The α_p grain in Fig. 4(a) was observed to deform by <a>-type a/3<$\bar{1}2\bar{1}0$> slip in the basal and prism planes. Another grain deforming by both basal and pyramidal slip is shown in bright field (BF) STEM in Fig. 4(b). In both Fig. 4(a) and (b), adjacent secondary alpha plates can be observed; in neither case was slip band transmission between an α_p grain and the neighbouring α_s/β region observed.

Table 2
Spatial and (0002) plane normal orientation to the loading direction of facets #1-#4 in Fig. 2, near the fatigue crack growth initiation site to the loading direction.

Facet	Orientation (deg.)	
	Spatial	(0002) plane normal
1	17.3	15.3
2	47.6	44.8
3	40.4	24.0
4	42.9	16.3

Please cite this article in press as: Joseph, S., et al., Slip transfer and deformation structures resulting from the low cycle fatigue of near-alpha titanium alloy Ti-6242Si, International Journal of Plasticity (2017), https://doi.org/10.1016/j.ijplas.2017.09.012

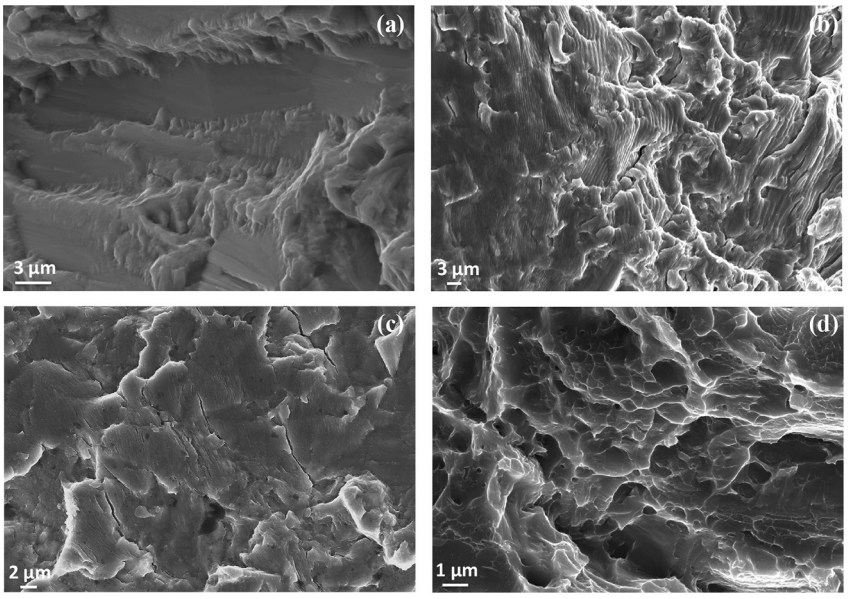


Fig. 3. SEM fractographs of the remainder of the fracture surface; (a) neighbouring facets around the fracture initiation region (b) fatigue striations (c) secondary cracks and (d) ductile microvoids.

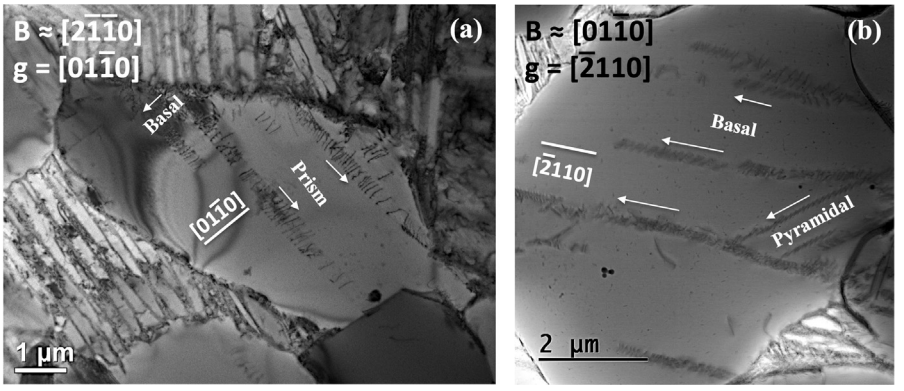


Fig. 4. (a) Bright field TEM image under two beam condition near the [2$\bar{1}\bar{1}$0] beam direction and (b) bright field STEM image near the [01$\bar{1}$0] beam direction showing slip activity in the α_p.

Slip transfer was studied between two grains of similar orientation within a microtextured region, with [10$\bar{1}$0] near the loading direction, Fig. 5(a). The crystallographic orientations of the grains are shown in the inset of the figure. Several slip systems were activated in these grains, with the inferred direction of dislocation movement shown by the arrows. The slip systems, which are transferred across the boundaries, are discussed here. The bright field TEM images under two beam condition in Fig. 5 show clearly the dislocation activities near the boundary. The diffraction conditions were selected separately in each grain to show the dislocation structure in each grain. These slip systems were analysed along four beam directions [2$\bar{1}\bar{1}$0], [10$\bar{1}$0], [7$\bar{2}\bar{5}$3] and [5$\bar{1}\bar{4}$3]. These electron beam conditions provide many g vectors such as [0002], [01$\bar{1}$0], [01$\bar{1}\bar{1}$], [01$\bar{1}\bar{2}$][$\bar{1}$013], [1$\bar{1}$03], [$\bar{1}\bar{2}\bar{1}$2] and [$\bar{1}\bar{2}\bar{1}\bar{4}$] for two beam condition to analyse the Burger's vector of the dislocations. The slip system A in grain 1 transfers across the boundary into grain 2 as slip system B. Similarly, the slip system C in grain 2 transfers into grain 3 as slip system D. Slip E in grain 3 impinged on the thin α_s+β region and nucleated dislocations F in the neighbouring grain from the point where it impinged. No strain contrast was observed across any boundaries of the grains investigated as the grains are oriented for easy slip transfer across the boundaries. Table 3 shows the Burger's vector, line direction and slip plane of the dislocations activated in the grains. The line directions of the dislocations indicate that they all possess screw character. <a_3> prism slip was activated in grains 1 and 2 and this slip directly transferred across the boundary. This can be clearly seen in Fig. 5 (b) and (c). Strain transfer occurred across the boundary between grains 3 and 4, Fig. 5(d) where one type of slip in grain 3 activated another type of slip in the neighbouring grain 4. <c+a_2>-type pyramidal slip in grain 3 impinge on the boundary and ejected dislocations of <a_3> type prism slip in grain 4. The compatibility between active

Please cite this article in press as: Joseph, S., et al., Slip transfer and deformation structures resulting from the low cycle fatigue of near-alpha titanium alloy Ti-6242Si, International Journal of Plasticity (2017), https://doi.org/10.1016/j.ijplas.2017.09.012

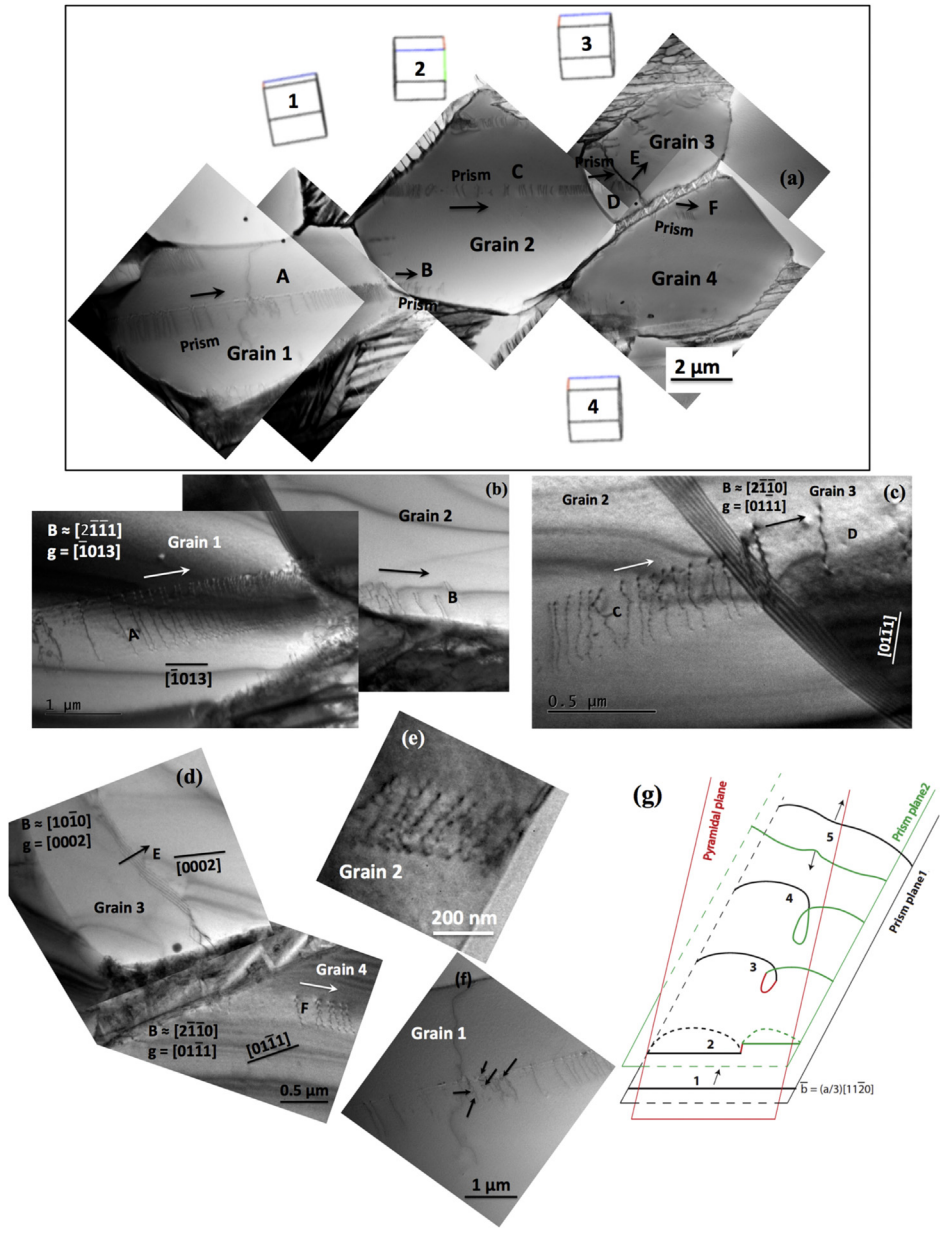


Fig. 5. (a) Bright field STEM image showing slip transfer across α_p grains with [10$\bar{1}$0] near to the loading direction and (b, c and d) bright field TEM images showing slip transfer across the grain boundary, under the two beam condition (e) Magnified view of the piled up dislocations at one end of the grain 2 (f) Magnified view of the dislocation activities at the center of grain 1 and (g) Schematic showing the dislocation generation by multiple cross-slip events. The loading direction is out of the plane of the figure.

Table 3
Burgers vector, line direction and slip plane for the slip systems observed in the soft grains of Fig. 5.

Grain	Slip System	Burgers vector	Line direction	Slip plane
1	A	(a/3)[11$\bar{2}$0]	[11$\bar{2}$0]	(1$\bar{1}$00)
2	B	(a/3)[11$\bar{2}$0]	[11$\bar{2}$0]	(1$\bar{1}$00)
	C	(a/3)[11$\bar{2}$0]	[11$\bar{2}$0]	(1$\bar{1}$00)
3	D	(a/3)[11$\bar{2}$0]	[11$\bar{2}$0]	(1$\bar{1}$00)
	E	(a/3)[1$\bar{2}$13]	[1$\bar{2}$13]	($\bar{1}$2$\bar{1}$2)
4	F	(a/3)[11$\bar{2}$0]	[11$\bar{2}$0]	(1$\bar{1}$00)

Please cite this article in press as: Joseph, S., et al., Slip transfer and deformation structures resulting from the low cycle fatigue of near-alpha titanium alloy Ti-6242Si, International Journal of Plasticity (2017), https://doi.org/10.1016/j.ijplas.2017.09.012

slip systems in adjacent grains was then checked by using a geometric compatability parameter m'. This Luster and Morris m' parameter for slip transfer is:

$$m' = \cos\phi . \cos\kappa$$

where ϕ is the angle between the normal to the slip planes and κ is the angle between the slip directions in the two grains. The m' value was calculated using Matlab toolbox STABiX (Mercier et al., 2015), Table 4. The m' values for the observed slip transfer are highlighted by squares. The m' values are greater than 0.9 for slip transfer across grain pairs 1/2 and 2/3, so the slip systems are well aligned for transmission across these boundaries. This value is not the highest for grain pair 1/2 since other factors, such as the resolved shear stress, and the CRSS, also play a role. For grain pair 3/4, strain transfer occurred without any apparent slip transfer. Hence the slip transfer parameter for the observed slip systems is also low. Hence direct slip transfer was observed across grains that share a similar orientation and are concurrently oriented with their c-axis perpendicular to the loading direction, i.e., soft grains. Even though grains 3 and 4 share a similar orientation, slip transfer was not observed, presumably owing to the presence of retained β and secondary α in the boundary.

In addition, two interesting observations were made on these grains. There is pile-up of dislocations on either side of the boundary in grains 1 and 2 and a non-basal <c+a> slip in grain 3. Pile up of dislocations on either side of the boundary is possible when the dislocation source emits dislocations in two opposite directions. Kacher et al. (Kacher and Robertson, 2016) observed this kind of dislocation generation in opposite directions during in-situ deformation studies on α-Ti. Multiple cross-slip events were responsible for the sequential emission of dislocations in opposite directions. Cross-slip in α-Ti was expected to occur predominantly between the prismatic and pyramidal planes as the core of <a> type screw dislocations are spread between the prismatic and the pyramidal planes (Naka and Lasalmonie, 1983). The possible mechanism for this type of dislocation generation is shown schematically in Fig. 5 (g). The dislocations are initially gliding on prism plane 1, which is

Table 4
Slip transfer parameter (m') for the soft grains analysed in Fig. 5.

Grain1

Grain 2	Bas	Pri1<a>	Pri2<a>	Pyr1<a>	Pyr1<c+a>	Pyr2<c+a>
Bas	0.96	0.14	0.15	0.58	0.38	0.42
Pri1<a>	0.14	0.93	0.91	0.88	0.43	0.31
Pri2<a>	0.15	0.91	0.93	0.87	0.44	0.31
Pyr1<a>	0.58	0.88	0.87	0.95	0.51	0.41
Pyr1<c+a>	0.38	0.43	0.44	0.51	0.96	0.98
Pyr2<c+a>	0.42	0.31	0.31	0.41	0.98	0.96

0.2 0.3 0.4 0.5 0.6 0.7 0.8 0.9

Grain 2

Grain 3	Bas	Pri1<a>	Pri2<a>	Pyr1<a>	Pyr1<c+a>	Pyr2<c+a>
Bas	0.99	0.08	0.08	0.55	0.33	0.36
Pri1<a>	0.08	0.99	0.80	0.91	0.32	0.25
Pri2<a>	0.08	0.80	0.99	0.74	0.41	0.25
Pyr1<a>	0.55	0.91	0.74	0.99	0.42	0.33
Pyr1<c+a>	0.33	0.32	0.41	0.41	0.99	0.94
Pyr2<c+a>	0.36	0.26	0.25	0.33	0.94	0.99

0.1 0.2 0.3 0.4 0.5 0.6 0.7 0.8 0.9

Grain 4

Grain 3	Bas	Pri1<a>	Pri2<a>	Pyr1<a>	Pyr1<c+a>	Pyr2<c+a>
Bas	1.00	0.02	0.02	0.50	0.27	0.30
Pri1<a>	0.02	1.00	0.78	0.89	0.26	0.22
Pri2<a>	0.02	0.78	1.00	0.69	0.37	0.21
Pyr1<a>	0.50	0.89	0.69	1.00	0.35	0.27
Pyr1<c+a>	0.27	0.26	0.36	0.35	1.00	0.91
Pyr2<c+a>	0.30	0.21	0.21	0.27	0.91	1.00

0.1 0.2 0.3 0.4 0.5 0.6 0.7 0.8 0.9

Please cite this article in press as: Joseph, S., et al., Slip transfer and deformation structures resulting from the low cycle fatigue of near-alpha titanium alloy Ti-6242Si, International Journal of Plasticity (2017), https://doi.org/10.1016/j.ijplas.2017.09.012

shown by position 1, and an arrow shows its direction of motion. A section of the dislocation cross-slipped, resulting in the formation of a sessile segment in the pyramidal plane, position 2. The colour of the dislocation segment indicates on which plane the dislocation segment resides. The segments on either side of the sessile segment then bowed under the applied stress (shown by dotted lines in position 2). The bowed out dislocations expand in their corresponding planes (position 3). Whereas the sessile segment on the cross-slipped plane would cross-slip back to the original glide plane or the plane parallel to the original glide plane (position 4), as the prism plane is the most energetically favourable plane for dislocation glide in α-Ti. Under the action of the applied stress, this segment expands into another dislocation in the direction opposite to the direction of motion of initial dislocation (position 5). Subsequently, another dislocation in the original glide plane would cross slip and generates another pair of dislocations moving in opposite directions. Thus the multiple cross-slip events would cause subsequent emission of dislocations in the opposite directions on different parallel prismatic planes. The slip traces in Fig. 5(e) shows that the dislocations in the slip band are gliding on different planes. Further, we were able to observe some dislocation cross-slip events, which are responsible for dislocation generation and dislocation debris resulting from these sequential cross-slip events (Fig. 5f) at the center of the grain, which supports the proposed mechanism. The cross-slip events and the dislocation loops resulting from the multiple cross-slip events are shown by arrows.

The non-basal <c+a> dislocations in grain 3 (slip system E) are geometrically and energetically unfavourable. However, it is possible when there is a formation of an attractive junction between glissile <a> and sessile <c> type dislocations (Yoo et al., 2001). As <a> type dislocations gliding by prism slip were observed in this grain, these <a> type dislocations are expected to forms junction with the pre-existing <c> type dislocations of the initial microstructure. The driving force for the junction formation comes from the long-range elastic interaction between <a> and <c> dislocations. This type of <c+a> dislocation generation was experimentally observed during in-situ deformation studies on a Ti alloy (Yu et al., 2013). The mobility of these dislocations is found to be low and their pile-up would significantly increase the work hardening of the material.

The incorporation of dislocations in an α_p grain into a grain boundary was also observed, Fig. 6. Many long dislocations were observed to be incorporated into the grain boundary, with no dislocation activity in the adjoining grain. These dislocations can dissociate into grain boundary dislocations and glide within the grain boundary plane. This requires that the grain boundary plane is a valid slip plane for these dislocations. Alternatively, the incorporated dislocations can disrupt the geometric structure of the grain boundary, potentially producing a transgranular crack that can pass unimpeded through the boundary (Lee et al., 1990b).

3.4.2. Deformation transfer between soft and hard oriented grains

A number of rogue grain pairs were investigated to understand the strain transfer mechanisms. Out of many pairs analysed, detailed analysis of a representative example is discussed here. The rogue grain pair presented here is a so-called soft grain, having its c-axis oriented approximately 90° to the loading axis, and a hard grain with its c-axis oriented approximately 13° from the loading axis, Fig. 7(a). The crystallographic orientation of the grain combination was obtained using EBSD on the TEM foil. The hexagonal crystals depict the orientation of the grains with respect to the loading axis. The grain boundary (g.b) is indicated by an arrow. The orientation relation of the grain pair was identified from selected area diffraction (SAD) patterns obtained from these grains when one of the grains was tilted to a zone axis. The SAD patterns of the hard and soft grains are shown in Fig. 8 where $[\bar{2}\underline{2}01]_{soft}//[\bar{1}2\bar{1}6]_{hard}$ and $(\bar{1}10\bar{4})_{soft}//(2\bar{2}01)_{hard}$. The strain transfer across the soft/hard grain boundary can be seen in Fig. 7(a). Slip systems A and B in the soft grain are piled-up against the grain boundary and slip systems C, D and E are activated in the hard grain. A higher magnification view is provided in Fig. 7(b). The incoming and outgoing dislocations were coincident for slip systems A/C but not for slip systems B/E and D. The pile-up of dislocations in slip systems A and B at the grain boundary generates a stress concentration and this stress is relieved by nucleating dislocations from the grain boundary for slip system C and away from the grain boundary for slip systems D and E. The primary slip system was slip system A; given the higher density of dislocations within this slip band we presume that this slip system was activated before

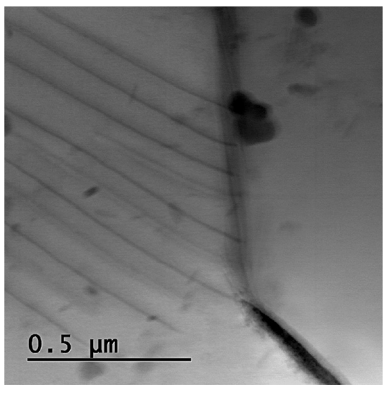


Fig. 6. Incorporation of dislocations in an α_p grain into a grain boundary.

Please cite this article in press as: Joseph, S., et al., Slip transfer and deformation structures resulting from the low cycle fatigue of near-alpha titanium alloy Ti-6242Si, International Journal of Plasticity (2017), https://doi.org/10.1016/j.ijplas.2017.09.012

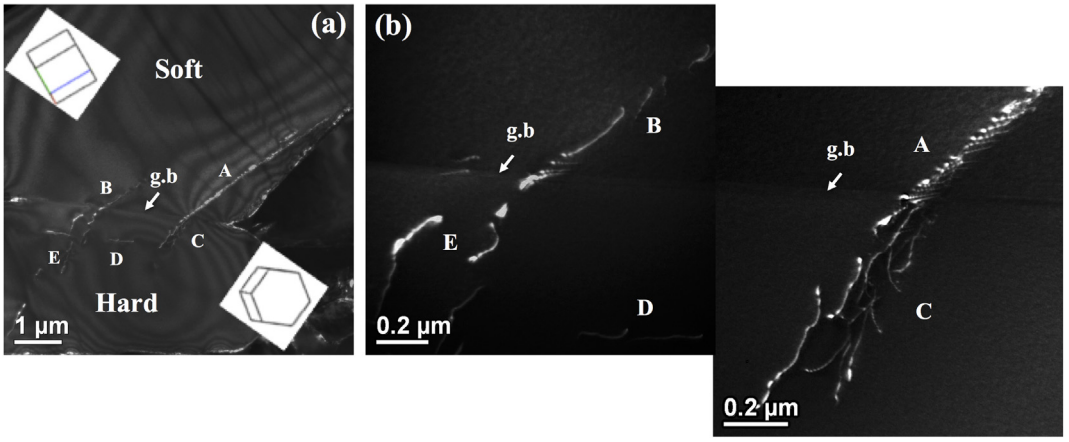


Fig. 7. Weak beam dark field image showing (a) strain transfer across soft/hard grain pair and (b) composite micrograph at high magnification. The loading direction is out of the plane of the figure.

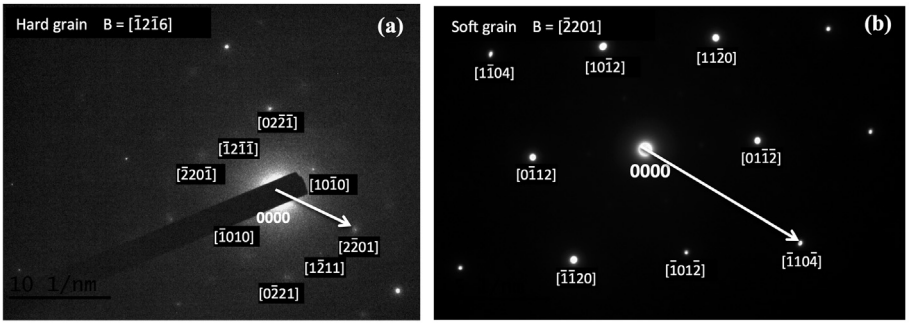


Fig. 8. SAD patterns from (a) hard and (b) soft grain when the soft grain was tilted to the [$\bar{2}201$] zone.

slip system B. The slip systems in the soft grain were analysed along four beam directions [$2\bar{1}\bar{1}0$], [$10\bar{1}0$], [$7\bar{2}\bar{5}3$] and [$5\bar{1}\bar{4}3$]. These directions provided many g vectors such as [0002], [$01\bar{1}0$], [$01\bar{1}1$], [$01\bar{1}\bar{2}$][$\bar{1}013$], [$1\bar{1}03$], [$\bar{1}2\bar{1}2$] and [$\bar{1}2\bar{1}4$] for two beam conditions to analyse the Burgers vector of the dislocations. The dislocations in the soft grain were identified as <a> type with a/3<$\bar{1}2\bar{1}0$> Burgers vector, according to the invisibility criterion under two beam condition. Slip occurred on the ($10\bar{1}0$) prismatic plane. The slip systems in the hard grain were analysed along four beam directions [0002], [$\bar{1}\bar{1}23$], [$\bar{1}012$] and [$\bar{2}113$]. These electron beams provided many g vectors such as [$10\bar{1}0$], [$01\bar{1}0$], [$\bar{1}100$], [$0\bar{1}\bar{1}\bar{1}$][$10\bar{1}1$], [$1\bar{1}01$], [$1\bar{2}10$], [$\bar{1}\bar{1}22$] and [$2\bar{2}01$] to analyse the Burgers vector. The dislocations in the hard grain were identified as <a> type with a/3 [$\bar{1}\bar{1}20$] Burgers vector. It was difficult to determine the slip plane of the dislocations in the hard grain, as the dislocations were not piled up on a particular plane and they were comparatively isolated dislocations.

The dislocation structures in the hard grain are complex, with different segments having different line directions. We have focussed on segments 1-9 marked in Fig. 9 (a and b), 3 segments in each slip system. The dislocation line ($\bar{u}$) determination is relatively simple if the habit plane of the dislocations is known, which is the case for the dislocations in the soft grain. As the habit plane is unknown for the dislocations in the hard grain, the dislocations are treated as isolated single dislocations and the procedure discussed by Edington (1974) was followed to determine the dislocation line direction in the hard grain. The dislocation line direction determination of dislocations in the soft and hard grains can be found in the Appendix. The stereographic analysis in Appendix shows that the dislocation segments 1, 3, 4, 6, 7 & 9 have the same line direction [$\bar{1}\bar{1}20$] and segments 2, 5 and 8 have a [$\bar{2}113$] direction. The Burgers vector and line direction of the dislocations in the soft and hard grain are shown in Table 5. It can be seen that the dislocations are of different types in the soft and hard grain. The case where a dislocation pile-up at a point in the grain boundary causes the activation of other types of dislocations in the adjacent grain, is the one of several possible strain transfer mechanisms discussed in the literature (Shen et al., 1986; Shen et al., 1988; Lee et al., 1990a,b).

The prism and pyramidal plane traces are shown in Fig. 9. First let us consider the dislocation segments 1-3 in slip system C. It is clear that all the dislocation segments are not gliding on a single plane. Segments 1 and 3 are close to the trace of the prism plane and are gliding on prism plane ($1\bar{1}00$) and segment 2 is close to the trace of pyramidal plane is gliding on pyramidal plane ($1\bar{1}01$). The line direction of these dislocation segments also supports this observation. Hence the dislocation cross slips during its movement. The schematic in Fig. 9(c) depicts the dislocation cross slip which can account for the features

Please cite this article in press as: Joseph, S., et al., Slip transfer and deformation structures resulting from the low cycle fatigue of near-alpha titanium alloy Ti-6242Si, International Journal of Plasticity (2017), https://doi.org/10.1016/j.ijplas.2017.09.012

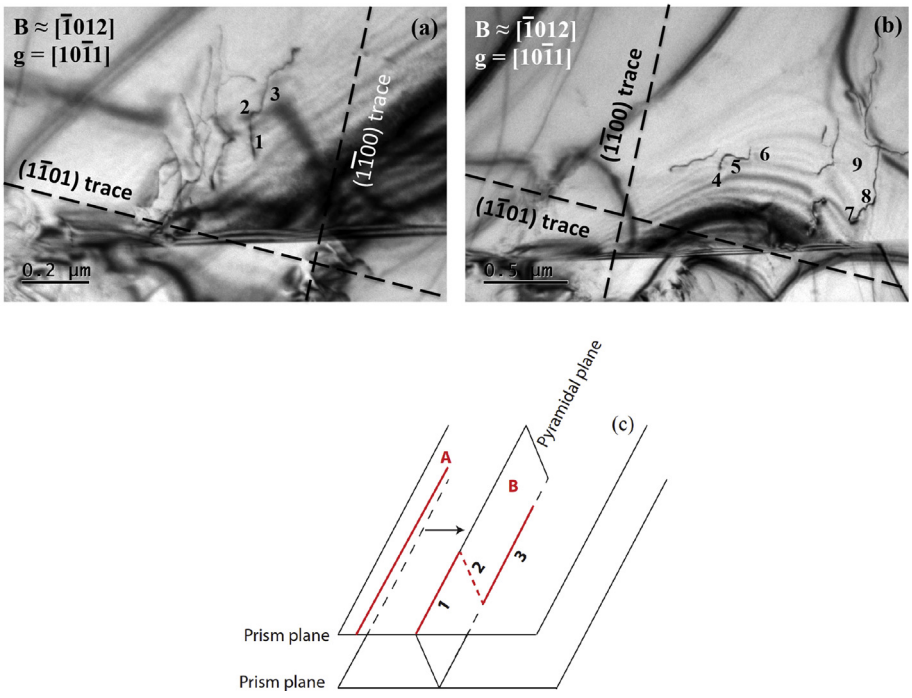


Fig. 9. Bright field image of dislocations in hard grain (a) slip system C and (b) slip systems D & E under the two beam condition, with beam direction B near [$\bar{1}$012] and (c) schematic showing dislocation cross-slip.

Table 5
Burgers vector and line direction of dislocations in the soft/hard grain pair of Fig. 7.

Slip System	Dislocation segment	Burgers vector	Line direction
Soft grain			
A		(a/3)[$\bar{1}$2$\bar{1}$0]	[$\bar{1}$2$\bar{1}$2]
B		(a/3)[$\bar{1}$2$\bar{1}$0]	[$\bar{1}$2$\bar{1}$2]
Hard grain			
C	1	(a/3)[$\bar{1}\bar{1}$20]	[$\bar{1}\bar{1}$20]
	2	(a/3)[$\bar{1}\bar{1}$20]	[$\bar{2}$113]
	3	(a/3)[$\bar{1}\bar{1}$20]	[$\bar{1}\bar{1}$20]

in the image. The dislocations with screw character are primarily gliding on the prism plane which is shown by position A and a small segment of the dislocation cross slips to a pyramidal plane. When this segment reaches the next prism plane, it leaves a segment with nearly edge character in the pyramidal plane, which is shown by position B. The segments 4-6 in slip D and segments 7-9 in slip E also show a similar type of cross slip.

Hence, the stress concentration due to the pile-up of dislocations in the soft grain activates dislocation sources in the hard grain rather than easing the passage of slip dislocations through the boundary. <a_3>-type dislocations nucleated in the hard grain due to the pile up of <a_2>– type dislocations in the soft grain. Dislocation sources might be activated either at the boundary or within the hard grain; both scenarios have been observed in this case (Fig. 7). The different type and nature of dislocation nucleation in the hard grain suggests that it is a strain transfer mechanism rather than slip transfer. The slip transfer parameter m' calculated for the soft/hard grain pair, Table 6, results in low m' values for the observed slip systems. Slip transfer across the boundary is necessarily difficult for hard/soft grain pairs since slip systems with high Schmid factors in a soft grain must have low Schmid factors in a hard grain. Once nucleated, dislocations in the hard grain multiply by cross slip; it is believed that cross slip is responsible for dislocation multiplication and patterning in fatigue (Suresh, 2004). Cross slip usually takes place under high stresses (Messerschmidt and Bartsch, 2003) and hence it can be inferred that the load imposed on the hard grain by the slip band in the soft grain must have been considerable. Further, the mobility of dislocations on the cross slip planes is lower than on the primary planes (Messerschmidt and Bartsch, 2003).

3.4.3. Dislocations in transformed β grains

The dislocation structures observed in the secondary alpha (α_s) are shown in Fig. 10. Random dislocation lines (Fig. 10a) and straight dislocations and dislocation loops (Fig. 10b) were observed in the α_s rather than dislocation arrays. Dislocation

Table 6
Slip transfer parameter (m') for the soft/hard grain pair of Fig. 7

Hard grain \ Soft grain	Bas	Pri1<a>	Pri2<a>	Pyr1<a>	Pyr1<c+a>	Pyr2<c+a>
Bas	0.15	0.75	0.91	0.73	0.78	0.85
Pri1<a>	0.79	0.32	0.28	0.61	0.88	0.80
Pri2<a>	0.84	0.28	0.32	0.56	0.97	0.86
Pyr1<a>	0.76	0.59	0.55	0.82	0.85	0.88
Pyr1<c+a>	0.82	0.79	1.00	0.83	0.94	0.85
Pyr2<c+a>	0.85	0.77	0.92	0.80	0.87	0.92

0.2 0.3 0.4 0.5 0.6 0.7 0.8 0.9

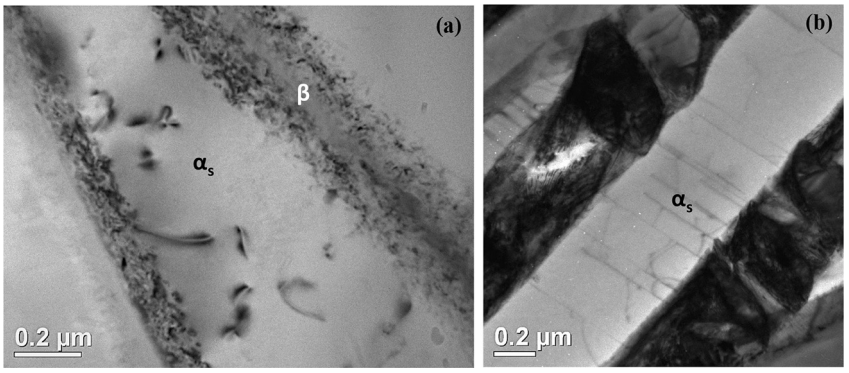


Fig. 10. (a) Random dislocation lines and (b) straight dislocations and dislocation loops in α_s.

bands and cavities observed in the β phase are shown in Fig. 11(a) and (b) respectively. These cavities are expected to form due to load shedding of the α_s plates onto the β plates (Embury and Hirth, 1994). Cavities in the retained β have previously been observed in Ti 6242 at the intersection of slip bands in the α_s (Gerland et al., 2009), and may be significant for fatigue behaviour. The interaction between the dislocations in the α_s and the β is shown in Fig. 11(c). Furthermore, a large number of dislocations were observed at the α_s/β boundary, Fig. 11(a) and (c), which was also observed in a sample examined prior to LCF loading. These dislocations are misfit dislocations generated during α precipitation due to the lattice mismatch between the two phases. In general, it appears that prism slip bands in the primary α find it difficult to produce slip in the transformed β regions, e.g. Fig. 4(a), and therefore it is interesting to observe that transformed β is probably favourable for the avoidance of the slip localization features and slip transfer associated with fatigue deformation.

3.5. Relevance of results to gas turbine operating regimes

Of course, gas turbines are subject to a great variety of loading regimes; mostly rotating parts are subjected to tension during operation and to zero stress between load cycles, but local areas around features, surface stress modification due to machining or shot peening, or the effect of stress relaxation around features, may lead to the fully spectrum of load ratios from −1 to 1. Titanium has been observed to display tension-compression asymmetry, and range-mean behaviours may also not be linear, depending on the microstructural form and specific alloy. In the present case the maximum stress was selected in order to provide an appropriate cyclic life, in the range of gas turbine flight cyclic life (10^4–10^5 cycles). Even then, it should be appreciated that component loading regimes will often be a superposition of vibrational, flight level and throttle-setting related loads, in addition to transients, and therefore an equivalence between LCF cycles and flights cannot necessarily be drawn.

4. Conclusions

Dislocation behaviour and slip transfer in Ti6242Si subject to low cycle fatigue has been investigated in this work and the following observations made.

Please cite this article in press as: Joseph, S., et al., Slip transfer and deformation structures resulting from the low cycle fatigue of near-alpha titanium alloy Ti-6242Si, International Journal of Plasticity (2017), https://doi.org/10.1016/j.ijplas.2017.09.012

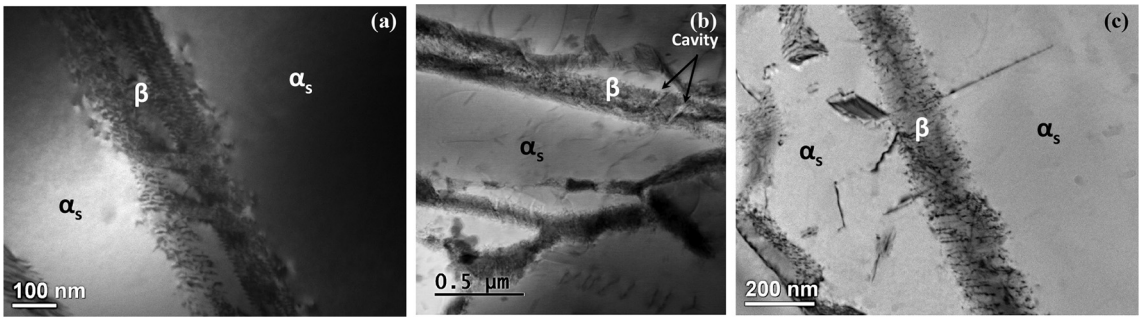


Fig. 11. (a) Dislocation bands in the β phase (b) Cavities in the β phase and (c) Dislocation interaction between α_s and β.

- The alloy mainly deforms by slip in α_p grains and this slip is found to be localized within the α_p grains in slip bands. Slip occurs by basal, prismatic and pyramidal slip.
- Direct slip transfer occurred in the soft grains within the microtextured region, where slip bands could cascade between grains of similar orientation. No strain contrast was observed across these boundaries as the slip alignment across the boundary was favourable. Multiple cross-slip events are responsible for dislocation generation in these grains.
- Some of the α_p dislocations were incorporated into the α_p grain boundary without the grain boundary responding by ejecting dislocations into the adjacent grain. This type of dislocation incorporation into a grain boundary can disturb the geometric structure of the grain boundary and result in formation of transgranular crack in the boundary.
- Alternatively, pile-up of dislocations in a soft-oriented grain was observed to activate dislocation sources in the neighbouring hard grain rather than easing the passage of dislocations through the boundary. A much smaller number of dislocations observed in the hard grain indicate that the hard grain did not undergo a significant plastic deformation. Those dislocations did not glide on well-defined slip planes. During multiplication, they change from one plane to another by cross slip.
- Straight dislocations, dislocation tangles and loops were observed in the α_s. In contrast, dislocation bands and even cavities were observed in the β ligaments due to dislocation interaction between the α_s and retained β.

Acknowledgements

The authors wish to acknowledge the contribution and useful discussions with Prof D Rugg at Rolls-Royce plc, Prof FPE Dunne and Dr TB Britton at Imperial, and Prof AJ Wilkinson in Oxford, with whom we are funded under the Hexmat EPSRC programme grant EP/K034332/1.

Appendix A. Supplementary data

Supplementary data related to this article can be found at 10.1016/j.ijplas.2017.09.012.

Appendix

Trace analysis shows that the habit plane of the dislocations in the soft grain is the $(10\bar{1}0)$ prismatic plane. The bright field image in Fig. A.1 (a) shows the dislocations in the soft grain when the foil normal is $[2\bar{1}\bar{1}0]$. The habit plane $(10\bar{1}0)$ of these dislocations intersects the $(2\bar{1}\bar{1}0)$ foil plane parallel to the [0002] direction with the projection of the dislocations into the diffraction pattern being $\approx 58^\circ$ anticlockwise from [0002]. From the stereographic projection shown in Fig. A.1 (b) the line direction $\bar{u}$ is deduced to be $[\bar{1}2\bar{1}2]$, which is neither parallel nor perpendicular to the Burgers vector of these dislocations. Hence these dislocations in the soft grain show mixed character.

The line direction of dislocation segments 1 to 9, which are marked in Fig. 9, was determined in the hard grain. As the segments 1, 3, 4, 6, 7 & 9 have the same line direction, the stereographic analysis is only shown for segment 1. Similarly, the line segments 2, 5 and 8 have the same line direction and the analysis is shown for segment 2. For this analysis, the images of dislocations were captured with three different beam directions. The images of dislocations under beam directions $[\bar{1}\bar{1}23]$, $[\bar{1}012]$ and $[\bar{2}113]$ are shown in Fig. A.2. The angle between the directions marked and the normal to the projected line direction of the dislocation was measured. The exact beam directions in Fig. A.2 were constructed in a stereogram, Fig. A.3. Directions A, B and C, normal to the direction of the dislocations were constructed by measuring the angles from the directions marked in Fig. A.2 along the greater circles corresponding to the values of the beam directions. The line direction $\bar{u}$ of each dislocation was then obtained by finding the pole of the great circle through these normals. Fig. A.3 shows the stereographic analysis for the line direction of the dislocation segments 1 and 2. The line directions are determined to be 8° from

Please cite this article in press as: Joseph, S., et al., Slip transfer and deformation structures resulting from the low cycle fatigue of near-alpha titanium alloy Ti-6242Si, International Journal of Plasticity (2017), https://doi.org/10.1016/j.ijplas.2017.09.012

$[\bar{1}\bar{1}20]$ for segment 1 and 6° from $[\bar{2}113]$ for segment 2 respectively. The accuracy of the method is ±5° when the beam directions are indexed with an error of <1°.

References

Anahid, M., Samal, M.K., Ghosh, S., 2011. Dwell fatigue crack nucleation model based on crystal plasticity finite element simulations of polycrystalline titanium alloys. J. Mech. Phy. Solids 59 (10), 2157–2176.
Bache, M.R., 2003. A review of dwell sensitive fatigue in titanium alloys: the role of microstructure, texture and operating conditions. Int. J. Fatigue 25, 1079–1087.
Bache, M.R., Evans, W.J., 2003. Dwell sensitive fatigue response of titanium alloys for power plant applications. J. Eng. Gas. Turb. Power 125 (1), 241–245.
Bache, M.R., Copet, M., Davies, H.M., Evans, W.J., Harrison, G., 1997a. Dwell sensitive fatigue in a near alpha titanium alloy at ambient temperature. Int. J. Fatigue 19 (93), 83–88.
Bache, M.R., Evans, W.J., Davies, H.M., 1997b. Electron back scattered diffraction (EBSD) analysis of quasi-cleavage and hydrogen induced fractures under cyclic and dwell loading in titanium alloys. J. Mat. Sci. 32 (13), 3435–3442.
Bantounas, I., Dye, D., Lindley, T.C., 2009. The effect of grain orientation on fracture morphology during high cycle fatigue of Ti-6Al-4V. Acta Mater 57 (12), 3584–3595.
Davidson, D.L., Eylon, D., 1980. Titanium alloy fatigue fracture facet investigation by selected area electron channeling. Metall. Trans. A 11, 837–843.
Dunne, F.P.E., Rugg, D., 2008. On the mechanisms of fatigue facet nucleation in titanium alloys. Fatigue Fract. engng. Mat. Struct. 31, 949–958.
Dunne, F.P.E., Walker, A., Rugg, D., 2007a. A systematic study of hcp crystal orientation and morphology effects in polycrystal deformation and fatigue. Proc. R. Soc. A 463, 1467–1489.
Dunne, F.P.E., Rugg, D., Walker, A., 2007b. Length scale-dependent, elastically anisotropic, physically-based hcp crystal plasticity: application to cold-dwell fatigue in Ti alloys. Int. J. Plast. 23, 1061–1083.
Edington, J.W., 1974. Electron Diffraction in the Electron Microscope (Vol. 2), Practical Electron Microscopy. The Macmillan Press Ltd, London and Basingstoke, pp. 57–58.
Embury, J.D., Hirth, J.P., 1994. On dislocation storage and the mechanical response of fine-scale microstructures. Acta Metall. Mater 42 (6), 2051–2056.
Evans, W.J., 1987. The influence of microstructure on dwell sensitive fatigue in a near alpha titanium alloy. Scr. Metall. 21 (4), 469–474.
Evans, W.J., Bache, M.R., 1994. Dwell-sensitive fatigue under biaxial loads in the near-alpha titanium-alloy IMI685. Int. J. Fatigue 16 (7), 443–452.
Eylon, D., Hall, J.A., 1977. Fatigue behaviour of beta processed titanium alloy IMI 685. Mater. Trans. A 8, 981–990.
Gerland, M., Lefranc, P., Doquet, V., Sarrazin-Baudou, C., 2009. Deformation and damage mechanisms in an α/β 6242 Ti alloy in fatigue, dwell-fatigue and creep at room temperature-Influence of internal hydrogen. Mat. Sci. Eng. A 507 (1–2), 132–143.
Germain, L., Gey, N., Humbert, M., Bocher, P., Jahazi, M., 2005. Analysis of sharp microtexture heterogeneities in a bimodal IMI 834 billet. Acta Mater 53, 3535–3543.
Germain, L., Gey, N., Humbert, M., Vo, P., Jahazi, M., Bocher, P., 2008. Texture heterogeneities induced by subtransus processing of near-α titanium alloys. Acta Mater 56 (16), 4298–4308.
Gey, N., Bocher, P., Uta, E., Germain, L., Humbert, M., 2012. Texture and microtexture variations in a near-α titanium forged disk of bimodal microstructure. Acta Mater 60 (6–7), 2647–2655.
Hack, J.E., Leverant, G.R., 1980. A model for hydrogen-assisted crack initiation on planar shear bands in near-alpha titanium alloys. Scr. Metall. 14, 437–441.
Hall, G.S., Seagle, S.R., Bomberger, H.B., 1973. In: Titanium Science and Technology, vol. 4. Plenum Press, New York, NY, p. 2141.
Hasija, V., Ghosh, S., Mills, M.J., Joseph, D.S., 2003. Deformation and creep modeling in polycrystalline Ti-6Al alloys. Acta Mater 51 (15), 4533–4549.
Honnorat, Y., 1996. Issues and breakthrough in the manufacture of turbo engine titanium parts. Mat. Sci. Eng. A 213, 115–123.
Kacher, J., Robertson, I.M., 2016. In situ TEM characterisation of dislocation interactions in α-titanium. Philos. Mag. 96 (14), 1437–1447.
Kassner, M.E., Kosaka, Y., Hall, J.S., 1999. Low-cycle dwell-time fatigue in Ti-6242. Mater. Trans. A 30, 2383–2389.
Kirane, K., Ghosh, S., 2008. A cold dwell fatigue crack nucleation criterion for polycrystalline Ti-6242 using grain-level crystal plasticity FE model. Int. J. Fatigue 30 (12), 2127–2139.
Le Biavant, K., Pommier, S., Prioul, C., 2002. Local texture and fatigue crack initiation in a Ti-6Al-4V titanium alloy. Fatigue Fract. Engng. Mat. Struct. 25, 527–545.
Lee, T.C., Robertson, I.M., Birnbaum, H.K., 1990a. An in situ transmission electron microscope deformation study of the slip transfer mechanisms in metals. Mater. Trans. A 21, 2473–2447.
Lee, T.C., Robertson, I.M., Birnbaum, H.K., 1990b. TEM in situ deformation study of the interaction of lattice dislocations with grain boundaries in metals. Phil. Mag. A 62 (1), 131–153.
McBagonluri, F., Akpan, E., Mercer, C., Shen, W., Soboyejo, W.O., 2005. An investigation of the effects of microstructure on dwell fatigue crack growth in Ti-6242. Mat. Sci. Eng. A 405 (1–2), 111–134.
Mercier, D., Zambaldi, C., Bieler, T.R., 2015. A Matlab toolbox to analyze slip transfer through grain boundaries, 17th International Conference on Textures of Materials (ICOTOM 17). IOP Conf Ser. Mater. Sci. Eng. 82, 012090. https://doi.org/10.1088/1757–1899X/82/1/012090.
Messerschmidt, U., Bartsch, M., 2003. Generation of dislocations during plastic deformation. Mat. Chem. Phy 81, 518–523.
Naka, S., Lasalmonie, A., 1983. Cross-slip on the first order pyramidal plane $(1\,0\bar{1}1)$ of a-type dislocations $[1\,\bar{2}\,1\,0]$ in the plastic deformation of a-titanium single crystals. J. Mat. Sci. 18, 2613–2617.
Pilchak, A.L., 2014. A simple model to account for the role of microtexture on fatigue and dwell fatigue lifetimes of titanium alloys. Scr. Mater 74, 68–71.
Qiu, J., Ma, Y., Lei, J., Liu, Y., Huang, A., Rugg, D., Yang, R., 2014. A comparative study on dwell fatigue of Ti-6Al-2Sn-4Zr-xMo (x = 2 to 6) alloys on a microstructure-normalized basis. Mater. Trans. A 45, 6075–6087.
Shen, Z., Wagoner, R.H., Clark, W.A.T., 1986. Dislocation pile-up and grain boundary interactions in 304 stainless steel. Scr. Metall. 20 (6), 921–926.
Shen, Z., Wagoner, R.H., Clark, W.A.T., 1988. Dislocation and grain boundary interactions in metals. Acta Metall. 36 (12), 3231–3242.
Shen, W., Soboyejo, W.O., Soboyejo, A.B.O., 2004. Microstructural effects on fatigue and dwell-fatigue crack growth in α/β Ti-6Al-2Sn-4Zr-2Mo-0.1Si. Mater. Trans. A 35, 163–187.
Sinha, V., Spowart, J.E., Mills, M.J., Williams, J.C., 2006a. Observations on the faceted initiation site in the dwell-fatigue tested Ti-6242 alloy: crystallographic orientation and size effects. Mater. Trans. A 37, 1507–1518.
Sinha, V., Mills, M.J., Williams, J.C., 2006b. Crystallography of fracture facets in a near-alpha titanium alloy. Mater. Trans. A 37, 2015–2026.
Sinha, V., Mills, M.J., Williams, J.C., 2007. Determination of crystallographic orientation of dwell-fatigue fracture facets in Ti-6242 alloy. J. Mat. Sci. 42, 8334–8341.
Suresh, S., 2004. Fatigue of Materials, second ed. Cambridge University Press.
Tal-Gutelmacher, E., Eliezer, D., 2005. The hydrogen embrittlement of titanium based alloys. J. Mater 57 (9), 46–49.
Tan, C., Li, X., Sun, Q., Xiao, L., Zhao, Y., Sun, J., 2015. Effect of α-phase morphology on low cycle fatigue behaviour of TC21 alloy. Inter. J. Fatigue 75, 1–9.
Terlinde, G., Duerig, T.W., Williams, J.C., 1983. Microstructure, tensile deformation, and fracture in aged Ti 10V-2Fe-3Al. Mater. Trans. A 14, 2101–2115.
Tien, J.K., Chesnutt, J.C., Boone, D.H., Goward, G.W., 1973. In: Titanium Science and Technology, vol. 4. Plenum Press, New York, NY, p. 2517.
Tympel, P.O., Lindley, T.C., Saunders, E.A., Dixon, M., Dye, D., 2016. Macrozones and dwell fatigue crack initiation in Ti-6Al-4V. In: Proceedings of the 13th World Conference on Titanium. TMS (The Minerals, Metals & Materials Society), pp. 985–991.
Venkatramani, G., Ghosh, S., Mills, M., 2007. A size-dependent crystal plasticity finite-element model for creep and load shedding in polycrystalline titanium alloys. Acta Mater 55 (11), 3971–3986.

Please cite this article in press as: Joseph, S., et al., Slip transfer and deformation structures resulting from the low cycle fatigue of near-alpha titanium alloy Ti-6242Si, International Journal of Plasticity (2017), https://doi.org/10.1016/j.ijplas.2017.09.012

Yoo, M.H., Agnew, S.R., Morris, J.R., Ho, K.M., 2001. Non-basal slip systems in HCP metals and alloys: source mechanisms. Mat. Sci. Eng. A 319–321, 87–92.
Yu, Q., Sun, J., Morris Jr., J.W., Minor, A.M., 2013. Source mechanism of non-basal <c+a> slip in Ti alloy. Scr. Mater 69, 57–60.
Zheng, Z., Balint, D.S., Dunne, F.P.E., 2016a. Dwell fatigue in two Ti alloys: an integrated crystal plasticity and discrete dislocation study. J. Mech. Phy. Solids 96, 411–427.
Zheng, Z., Balint, D.S., Dunne, F.P.E., 2016b. Discrete dislocation and crystal plasticity analyses of load shedding in polycrystalline titanium alloys. Int. J. Plast. 87, 15–31.

Please cite this article in press as: Joseph, S., et al., Slip transfer and deformation structures resulting from the low cycle fatigue of near-alpha titanium alloy Ti-6242Si, International Journal of Plasticity (2017), https://doi.org/10.1016/j.ijplas.2017.09.012